Received: 4 April 2022 | Revised: 14 June 2022 | Accepted: 5 August 2022

DOI: 10.1002/cac2.12352

CANCER COMMUNICATIONS Open Access

LETTER TO THE EDITOR

miR-99a-5p modulates doxorubicin resistance via the COX-2/ABCG2 axis in triple-negative breast cancer: from the discovery to in vivo studies

Dear Editor,

Breast cancer (BC) is the most commonly diagnosed cancer and the fifth cause of cancer-related death worldwide [1]. Despite the advances in BC targeted therapies, cytotoxic chemotherapy is still widely used [2]. However, around 20%-30% of BC patients develop metastasis after treatment as a consequence of drug resistance [3]. In this context, microRNAs have emerged as potential therapeutic targets to overcome therapy resistance [4]. Therefore, we aimed to elucidate the molecular mechanisms underlying resistance to doxorubicin, one of the most effective chemotherapeutic agents used in BC. Methods are detailed in Supplementary Materials.

To identify miRNAs involved in doxorubicin resistance, the miRNA expression profiles of MDA-MB-231R cells with acquired doxorubicin resistance and their parental cell line MDA-MB-231 were compared (Supplementary Figure S1A). miR-99a-5p was found as the most differentially expressed miRNA, being downregulated in resistant cells (fold change = -17.83, $P = 0.027$) (Figure 1A).

We previously described miR-99a-5p as a good diagnostic biomarker downregulated in BC tissues when compared to healthy breast tissues [5]. To determine its clinical relevance in BC, we examined the association between miR-99a-5p expression and distant relapse-free survival (DRFS) in a cohort of 210 BC patients (GSE22216). miR-99a-5p was overexpressed in patients free of progression ($n = 131$) compared to patients with distant relapse ($n = 79$) (fold change = 1.72; $P = 0.019$), and its low expression was associated with shorter DRFS ($P = 0.004$; Supplementary Figure S1B-C). Additionally, its association with overall survival (OS) was assessed in the Molecular Taxonomy of Breast Cancer International Consortium (METABRIC, $n = 1262$) and The Cancer Genome Atlas (TCGA) cohorts ($n = 1062$), which confirmed that low miR-99a-5p expression was associated with poor prognosis (Supplementary Figure S1D-E).

Therefore, we hypothesized that miR-99a-5p could increase doxorubicin sensitivity. miR-99a-5p was described to increase sensitivity to radiation and cisplatin [6, 7], but its role in doxorubicin resistance was still unexplored. We demonstrated that miR-99a-5p overexpression decreased the half-maximal inhibitory concentration (IC_{50}) of doxorubicin (Figure 1B) and increased doxorubicin-induced apoptosis in MDA-MB-231 and MDA-MB-231R cells (Supplementary Figure S1F-G).

To elucidate the molecular mechanism by which miR-99a-5p sensitizes cells to doxorubicin, we compared the gene expression profiles of MDA-MB-231R and MDA-MB-231 cells by microarray analysis. To identify potential miR-99a-5p targets, mRNAs significantly upregulated in MDA-MB-231R cells were selected (Supplementary Figure S2A) and compared with predicted miR-99a-5p

Abbreviations: ABCG2, ATP-binding cassette subfamily G member 2; ALT, alanine transaminase; AST, aspartate aminotransferase; ATCC, American Type Culture Collection; BC, breast cancer; BET, Brunauer–Emmett–Teller; BJH, Barret-Joyner-Halenda; CI, confidence interval; COX-2, cyclooxygenase-2; CRE, creatinine; CTAB, Cetyltrimethylammonium bromide; DAPI, 4',6-diamidino-2-phenylindole; DLS, dynamic light scattering; DRFS, distant-relapse free survival; FDR, false discovery rate; FTIR, Fourier-transform infrared; GEO, Gene Expression Omnibus; H&E, hematoxylin and eosin; H&E, hematoxylin and eosin; HA, hyaluronic acid; HR, hazard ratio; IC_{50}, half-maximal inhibitory concentration; ICP-MS, inductively coupled plasma mass spectrometry; METABRIC, Molecular Taxonomy of Breast Cancer International Consortium; MFI, mean fluorescence intensity; MSNs, mesoporous silica nanoparticles; myh7, Myosin Heavy Chain 7; NCBI, National Center for Biotechnology Information; OS, overall survival; PEI, polyethyleneimine; PTFE, polytetrafluoroethylene; PXRD, Powder X-ray diffraction; qRT-PCR, quantitative real-time PCR; RIPA, radioimmunoprecipitation; RNU43, U43 Small Nuclear RNA; SAED, selected area electron diffraction; SD, standard deviation; SDS-PAGE, sodium dodecyl sulfate–polyacrylamide gel electrophoresis; SEM, standard error of the mean; siRNAs, short interfering RNAs; TCGA, The Cancer Genome Atlas; TEM, transmission electron microscopy; TEOS, tetraethylorthosilicate; TGA, thermogravimetric analysis; TMAH, tetramethylammonium hydroxide solution; TNBC, triple-negative breast cancer; URE, urea; UTR, untranslated region.

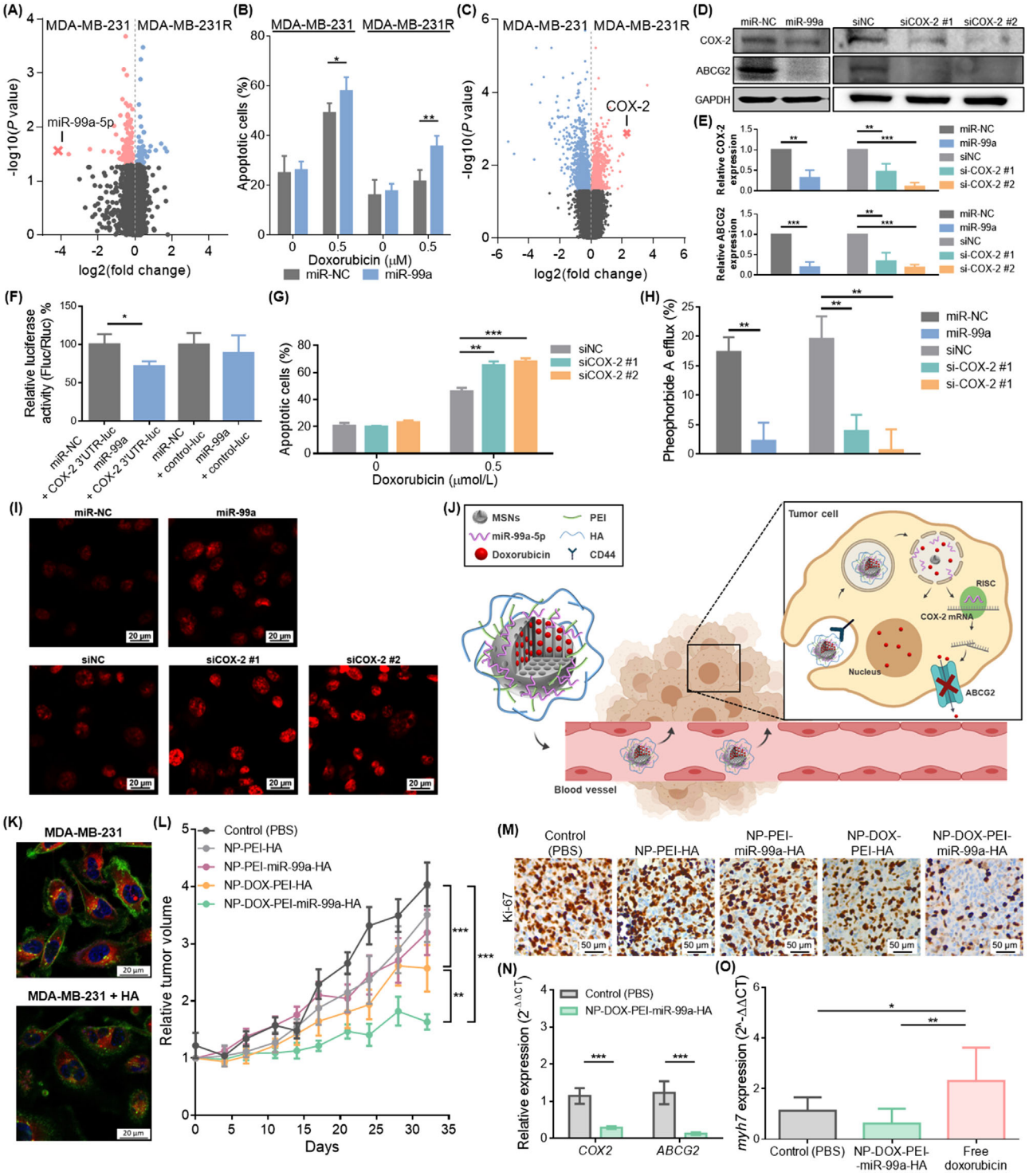

FIGURE 1 miR-99a-5p increases doxorubicin sensitivity through downregulation of COX-2 and ABCG2. (A) Volcano plot representing array results (Affymetrix GeneChip miRNA 4.0). Red dots represent miRNAs significantly upregulated in MDA-MB-231 cells, blue dots represent miRNAs significantly upregulated in MDA-MB-231R cells, and the cross symbol represents miR-99a-5p. (B) MDA-MB-231 and MDA-MB-231R cells were transfected with scramble miRNA (miR-NC) or miR-99a-5p (miR-99a), treated with 0.5 μmol/L doxorubicin for 48 hours, and evaluated for apoptosis by flow cytometry after FITC-Annexin V staining. Untreated cells were included as a control (mean ± SD). (C) Volcano plot representing array results (Affymetrix Clariom S array). Red dots represent mRNAs significantly upregulated in MDA-MB-231R cells, blue dots represent mRNAs significantly upregulated in MDA-MB-231 cells, and the cross symbol represents COX-2. (D-E) MDA-MB-231 cells were transfected with miR-NC, miR-99a, silencer negative control (siNC), or the COX-2 siRNAs (siCOX-2 #1 and siCOX-2 #2), and evaluated for expression levels of COX-2 and ABCG2 by Western blotting. Representative Western blotting images (D) and quantification (mean ± SD) (E). (F) Luciferase activity assays of HEK293T cells co-transfected with miR-NC or miR-99a and the luciferase vector containing 3'UTR of COX-2 or control luciferase vector (mean ± SD). (G) MDA-MB-231 cells were transfected with siNC, siCOX-2 #1, or

targets from miRWalk 2.0 (Supplementary Table S1). We found cyclooxygenase-2 (*COX-2*) as a potential target with the highest differential expression (fold change = 4.94; $P = 0.001$) (Figure 1C), and proved its upregulation in MDA-MB-231R cells (Supplementary Figure S2B-C). COX-2 is implicated not only in inflammation but also in tumorigenesis, treatment resistance, and poor prognosis in cancer patients [8].

To clarify whether miR-99a-5p modulates doxorubicin sensitivity through COX-2, we confirmed that miR-99a-5p overexpression inhibited *COX-2* expression and that it is a direct target of miR-99a-5p (Figure 1D-F, Supplementary Figure S2D). Then, we corroborated that COX-2 downregulation sensitized BC cells to doxorubicin, as it reduced IC_{50} values (Supplementary Figure S2E-F) and increased doxorubicin-induced apoptosis (Figure 1G).

The ATP-binding cassette subfamily G member 2 (ABCG2), a transporter involved in doxorubicin efflux, was suggested to be regulated by COX-2 [9]. Hence, we hypothesized that ABCG2 could be a downstream target of miR-99a-5p through COX-2. We found that miR-99a-5p downregulated the expression of ABCG2 (Figure 1D-E, Supplementary Figure S3A) and decreased the efflux of the ABCG2-specific substrate pheophorbide A (Figure 1H), thus confirming an inhibitory effect on ABCG2 activity. Besides, we proved that overexpression of miR-99a-5p increased the intracellular accumulation of doxorubicin (Figure 1I, Supplementary Figure S3B). Despite ABCG2 being listed as a predicted target of miR-99a-5p by miRWalk 2.0, luciferase reporter gene assay showed no direct interaction (Supplementary Figure S3C). Therefore, we proposed COX-2 as a link between miR-99a-5p and ABCG2. Our results evidenced that silencing of COX-2 downregulated ABCG2 (Figure 1D,E, Supplementary Figure S3D), reduced the pheophorbide A efflux (Figure 1H), and increased the intracellular accumulation of doxorubicin (Figure 1I, Supplementary Figure S3B). Besides, ABCG2 was upregulated in MDA-MB-231R cells (Supplementary Figure S3E-F). Collectively, these data suggest that miR-99a-5p increased sensitivity to doxorubicin in part by modulation of ABCG2 through COX-2.

To translate our findings, we designed mesoporous silica nanoparticles (MSNs) to deliver a combination of miR-99a-5p and doxorubicin to tumor cells. MSNs were loaded with doxorubicin and capped with consecutive layers of polyethyleneimine (PEI), miR-99a-5p, and hyaluronic acid (HA) (NP-DOX-PEI-miR-99a-HA) (Supplementary Figure S4A). PEI favors lysosomal escape, which is necessary to ensure the miRNA delivery into the cytoplasm, and HA is a biocompatible molecule that acts as a cap, inhibiting the release of the nanoparticle's content before internalization by cells, and targets CD44, which plays an important role in BC drug resistance (Figure 1J). Empty nanoparticles (NP-PEI-HA), nanoparticles containing only miR-99a-5p (NP-PEI-miR-99a-HA), or only doxorubicin (NP-DOX-PEI-HA) were evaluated as controls.

Nanoparticles were characterized by standard techniques that confirmed their successful preparation (Supplementary Figure S4B-H, Supplementary Table S2). The amount of encapsulated doxorubicin in NP-DOX-PEI-miR-99a-HA (70 mg/g SiO_2) was determined by thermogravimetric analyses and high-performance liquid chromatography. Besides, we verified that doxorubicin was released in lysosomal extract, whereas there was a very low delivery in phosphate-buffered saline (Supplementary Figure S4I), thus indicating that nanoparticles would deliver their content in lysosomes after being uptaken by cells. Moreover, the capacity of NP-DOX-PEI-miR-99a-HA to specifically target CD44 was confirmed by a competition

siCOX-2 #2, treated with doxorubicin (0.5 μmol/L) for 48 hours, and evaluated for apoptosis by flow cytometry after FITC-Annexin V staining. Untreated cells were included as a control (Mean ± SD). (H) MDA-MB-231 cells were transfected, and the percentage of pheophorbide A efflux was measured by flow cytometry to evaluate ABCG2 activity (mean ± SD). (I) After transfection, MDA-MB-231 cells were incubated with doxorubicin (5 μmol/L) for 3 hours at 37°C, and intracellular accumulation of doxorubicin was evaluated by fluorescence microscopy. Representative images are presented. (J) After intravenous injection, NP-DOX-PEI-miR-99a-HA passively targets tumors by the enhanced permeability and retention effect, whereas HA actively targets CD44 receptor in tumor cells. After cellular uptake, PEI induces disruption of lysosomal membranes, thereby delivering miR-99a-5p and doxorubicin into the cytoplasm. (K) Internalization of NP-DOX-PEI-miR-99a-HA in MDA-MB-231 and MDA-MB-231 cells pretreated with HA (5 mg/mL) for 30 minutes (MDA-MB-231+ HA) after 15-minute exposure to nanoparticles (25 μg/mL). Representative confocal microscopy images are presented (blue: nuclei; red: NP-DOX-PEI-miR-99a-HA; green: plasma membrane). (L) MDA-MB-231 cells were injected into the mammary fat pad of BALB/C mice. When the tumor size reached approximately 50 mm^3, mice ($n = 10$ per group) were treated 3 times per week with 10 mg/kg of nanoparticles for one month. Tumor growth curve (mean ± SEM). (M) Representative images of immunohistochemical staining of Ki-67 of paraffin-embedded xenograft sections. (N) *COX-2* and *ABCG2* expression in xenografts determined by qRT-PCR (mean ± SEM). (O) *myh7* expression in heart tissues determined by qRT-PCR (mean ± SEM). *$P < 0.05$; ** $P < 0.01$; *** $P < 0.001$. Abbreviations: ABCG2, ATP-binding cassette subfamily G member 2; COX-2, cyclooxygenase-2; HA, hyaluronic acid; myh7, Myosin Heavy Chain 7; miR-NC, miRNA negative control; PBS, phosphate-buffered saline; PEI, polyethyleneimine; qRT-PCR, quantitative real-time PCR; RISC, RNA-induced silencing complex; SD, standard deviation; SEM, standard error of the mean; siNC, siRNA negative control; UTR, untranslated region

assay. Pretreatment of MDA-MB-231 cells with free HA inhibited the uptake of nanoparticles (60.5%, $P < 0.001$) (Figure 1K, Supplementary Figure S4J), thus evidencing the NP-DOX-PEI-miR-99a-HA targeting to CD44.

We next examined the in vivo efficacy of the designed nanoparticles in a murine orthotopic xenograft model of triple-negative BC (TNBC). NP-DOX-PEI-miR-99a-HA induced the highest inhibition of tumor growth and cell proliferation; NP-PEI-HA and NP-PEI-mir-99a-HA displayed no significant differences with control, and NP-DOX-PEI-HA showed a moderate capacity to inhibit tumor growth (Figure 1L-M, Supplementary Figure S5A). Two days after last treatment, the tumor volume inhibition rates by NP-DOX-PEI-HA and NP-DOX-PEI-miR-99a-HA were 36.3% and 59.5%, respectively. Furthermore, the functional effect of miR-99a-5p was confirmed as COX-2 and ABCG2 were downregulated in tumors treated with NP-DOX-PEI-miR-99a-HA (Figure 1N). Biodistribution studies evidenced the ability of nanoparticles to target tumors, yet were also found in the kidneys, lungs, spleen, and liver (Supplementary Figure S5B). Moreover, nanoparticles had no toxicity in vivo (Supplementary Figure S5C-D).

Cardiotoxicity is the major adverse effect of doxorubicin [10]. To assess the potential benefit of doxorubicin encapsulation in combination with miR-99a-5p, doses of free doxorubicin and NP-DOX-PEI-miR-99a-HA with similar therapeutic efficacy were selected. Mice were treated with 1.6 mg/kg of free doxorubicin, whereas the equivalent dose of doxorubicin in nanoparticles was approximately 0.7 mg/kg, (44.0% of free drug) (Supplementary Figure S5E). Besides, higher levels of the marker of cardiac atrophy *myh7* (myosin heavy chain 7) (Figure 1O) and the presence of cytoplasmic vacuoles in cardiac tissue (Supplementary Figure S5F) evidenced that free doxorubicin induced cardiotoxicity, while NP-DOX-PEI-miR-99a-HA showed no differences with the control. These experiments proved the nanoparticles' ability to diminish the required dose of doxorubicin and the consequent cardiotoxicity.

In conclusion, we have shown that miR-99a-5p modulated doxorubicin resistance in TNBC. To translate our findings, we designed a nanoparticle for specific co-delivery of miR-99a-5p and doxorubicin that demonstrated its therapeutic potential in vivo, being more effective and less toxic than free doxorubicin alone.

DECLARATIONS

ACKNOWLEDGMENTS

We are especially grateful to the associations Amunt Contra el Cáncer, Asociación de la Lucha Contra el Cáncer de Montesa, and Corazón Solidario Contra el Cáncer. Funding for open access charge: Universitat Politècnica de València.

CONFLICT OF INTERESTS

The authors declare no conflict of interests.

FUNDING INFORMATION

This work was supported by Spanish Government and co-financed by FEDER Funds (PI18/01219, PI21/01351, PI18/00382, and RTI2018-100910-B-C41), CIBER-BBN (CB07/01/2012), CIBERONC (CB16/12/00481) and the Generalitat Valenciana (project PROMETEO 2018/024). I.G.-C. was funded by Generalitat Valenciana (ACIF/2016/030), A.A. and A.L. were funded by Asociación Española Contra el Cancer. J.F.B., was funded by Instituto de Salud Carlos III and the European Social Fund for the financial support "Sara Borrell" (CD19/00038), V.C.-N., was funded by Ministerio de Ciencia e Innovación (FPU grant), and J.M.C. was funded by Sociedad Española de Oncología Médica (Río Hortega-SEOM).

AUTHOR CONTRIBUTIONS

IGC: Conceptualization, methodology, data analysis, writing—original draft preparation. AAA, AL (Ana Lameirinhas), JFB, VCN, FR, SZ, JMG: Methodology, data analysis. AL (Ana Lluch), BB: Conceptualization, funding acquisition. FS: data acquisition and analysis. JMC, RMM, PE: Supervision, conceptualization, writing—reviewing and editing, funding acquisition.

ETHICS APPROVAL AND CONSENT TO PARTICIPATE

All animal experiments were approved by the Institutional Review Board of Biomedical Research Institute INCLIVA (Valencia, Spain) (2020/VSC/PEA/0131).

CONSENT FOR PUBLICATION

Not applicable.

DATA AVAILABILITY STATEMENT

The raw data required to reproduce these findings are available from the authors upon request.

Iris Garrido-Cano[1,2]
Anna Adam-Artigues[1]
Ana Lameirinhas[1]
Juan F. Blandez[2,3,4,5]
Vicente Candela-Noguera[3]
Federico Rojo[6,7]
Sandra Zazo[7]
Juan Madoz-Gúrpide[7]
Ana Lluch[1,6,8,9]
Begoña Bermejo[1,6,8]
Felix Sancenón[2,3,4,5]
Juan Miguel Cejalvo[1,6,8]

Ramón Martínez-Máñez[2,3,4,5]
Pilar Eroles[1,6,10]

[1]*Biomedical Research Institute INCLIVA, Valencia 46010, Spain*
[2]*Bioengineering, Biomaterials and Nanomedicine Networking Biomedical Research Centre (CIBER-BBN), Madrid 28029, Spain*
[3]*Interuniversity Research Institute for Molecular Recognition and Technological Development (IDM), Polytechnic University of Valencia, University of Valencia, Valencia 46010, Spain*
[4]*Joint Unit CIPF-UPV of Mechanisms of Diseases and Nanomedicine, Valencia, Polytechnic University of Valencia, Prince Felipe Research Center, Valencia 46012, Spain*
[5]*Joint Research Unit in Nanomedicine and Sensors, Polytechnic University of Valencia, Medical Research Institute Hospital La Fe, Valencia 46026, Spain*
[6]*Biomedical Research Networking Center in Oncology (CIBERONC), Madrid 28029, Spain*
[7]*Department of Pathology, Fundación Jiménez Díaz University Hospital Health Research Institute, Madrid 28040, Spain*
[8]*Department of Clinical Oncology, University Clinical Hospital of Valencia, Valencia 46010, Spain*
[9]*Department of Medicine, University of Valencia, Valencia 46010, Spain*
[10]*Department of Physiology, University of Valencia, Valencia 46010, Spain*

Correspondence
Pilar Eroles and Juan Miguel Cejalvo, Biomedical Research Institute INCLIVA, 46010 Valencia, Spain.
Email: pilar.eroles@uv.es; jmcejalvo@incliva.es

Ramón Martínez-Máñez, Bioengineering, Biomaterials and Nanomedicine Networking Biomedical Research Centre (CIBER-BBN), 28029 Madrid, Spain.
Email: rmaez@qim.upv.es

ORCID

Iris Garrido-Cano https://orcid.org/0000-0002-1211-473X

REFERENCES

1. Sung H, Ferlay J, Siegel RL, Laversanne M, Soerjomataram I, Jemal A, et al. Global Cancer Statistics 2020: GLOBOCAN Estimates of Incidence and Mortality Worldwide for 36 Cancers in 185 Countries. CA Cancer J Clin. 2021;71:209–49.
2. Waks AG, Winer EP. Breast Cancer Treatment: A Review. JAMA. 2019;321:288–300.
3. Tevaarwerk AJ, Gray RJ, Schneider BP, Smith ML, Wagner LI, Fetting JH, et al. Survival in patients with metastatic recurrent breast cancer after adjuvant chemotherapy: Little evidence of improvement over the past 30 years. Cancer. 2013;119:1140–8.
4. Si W, Shen J, Zheng H, Fan W. The role and mechanisms of action of microRNAs in cancer drug resistance. Clin Epigenetics. 2019;11:25.
5. Garrido-Cano I, Constâncio V, Adam-Artigues A, Lameirinhas A, Simón S, Ortega, B, et al. Circulating miR-99a-5p Expression in Plasma: A Potential Biomarker for Early Diagnosis of Breast Cancer. Int J Mol Sci. 2020;21:7427.
6. Mueller AC, Sun D, Dutta A. The miR-99 family regulates the DNA damage response through its target SNF2H. Oncogene. 2013;32:1164–72.
7. Zhang Y, Xu W, Ni P, Li A, Zhou J, Xu S. MiR-99a and miR-491 regulate cisplatin resistance in human gastric cancer cells by targeting CAPNS1. Int J Biol Sci. 2016;12:1437–47.
8. Goradel NH, Najafi M, Salehi E, Farhood B, Mortezaee K. Cyclooxygenase-2 in cancer: A review. J Cell Physiol. 2019;234:5683–99.
9. Kalalinia F, Elahian F, Behravan J. Potential role of cyclooxygenase-2 on the regulation of the drug efflux transporter ABCG2 in breast cancer cell lines. J Cancer Res Clin Oncol. 2011;137:321–30.
10. de Souza TF, Silva TQ, Costa FO, Shah R, Neilan TG, Velloso L, et al. Anthracycline Therapy Is Associated With Cardiomyocyte Atrophy and Preclinical Manifestations of Heart Disease. JACC Cardiovasc Imaging. 2018;11:1045–55.

SUPPORTING INFORMATION

Additional supporting information can be found online in the Supporting Information section at the end of this article.